

P1C.9 EQUATORIAL KELVIN WAVE PROPAGATION PAST SUMATRA: JUNE 2006 CASE ANALYSIS AND FORECAST SENSITIVITY EXPERIMENTS WITH COAMPS[®]

James A. Ridout * and Maria K. Flatau
Naval Research Laboratory, Monterey, California

1. INTRODUCTION

A recent paper by Inness and Slingo (2006) provides a brief overview of suggested mechanisms of interaction of the Madden Julian Oscillation (MJO) (e.g., Madden and Julian 1971, 1972, 1994; Hayashi and Sumi 1986; Hendon 1988; Chen et al. 1996; Zhang 2005) with the Maritime Continent. In addition, the authors present results from general circulation model experiments in which various idealized representations of the Maritime Continent were added to an aqua-planet version of the Hadley Centre coupled model. The effectiveness of the island of Sumatra in blocking the Kelvin wave signal of the MJO is particularly noted. This observation highlights the question as to the degree to which the island effectively blocks the MJO in nature, or perhaps blocks Kelvin waves of incipient MJOs. As a step towards better understanding this issue and the challenges of modeling wave propagation past Sumatra in short-medium range weather forecasts (M. Flatau) with the Navy Operational Global Atmospheric Prediction System (NOGAPS, Hogan et al. 1991), the present work focuses on analysis and forecasting of two equatorial Kelvin waves in the eastern Indian Ocean that occurred several days apart during June 2006. The waves are investigated in wind analyses carried out for the Indian Ocean region and in corresponding Tropical Rainfall Measuring Mission (TRMM) (e.g., Simpson et al. 1988; Schumacher and Houze 2000) rainfall data, focusing on their passage past Sumatra. The wind analyses and forecast experiments described here were carried out using the Coupled Ocean/Atmosphere Mesoscale Prediction System (COAMPS[®]) (Hodur 1997; Chen et al. 2003).

2. DATA PREPARATION

2.1 Wave Identification

The two June 2006 Kelvin waves examined in this study were identified by means of their signature in a Hovmöller diagram (Fig. 1) for the “equatorial” band from 0 – 10°N of TRMM rainfall data filtered to exclude westward propagating signals. The chosen latitudinal band is based on examination of both the TRMM data and wind

field data (see below), which showed that convection within the Kelvin wave tended to be shifted northward, off the equator, during this monsoon season period of study. The observed shift is consistent with the approximate 5 degree northward shift noted by Chatterjee and Goswami (2004) in equatorial Rossby waves during the summertime in the eastern Indian Ocean, apparently in response to a shift in the latitude of low-level zero absolute vorticity.

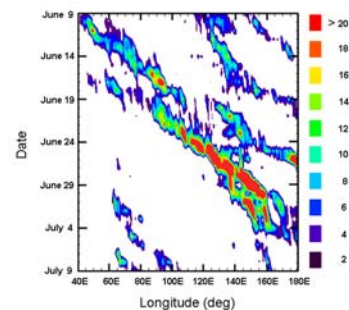


Fig. 1. Hovmöller diagram representing the latitudinal band 0 – 10°N for 9 June – 9 July 2006, showing TRMM rainfall rates (mm day⁻¹) filtered to exclude westward propagating signals.

The convective signal associated with each of the waves is first observed in the western Indian Ocean, where the second wave appears five days after the first. Applying the dispersion analysis of Wheeler and Kiladis (1990), it is somewhat difficult to distinguish these waves from the MJO, though by that analysis they appear to be slow Kelvin waves rather than fast-moving MJOs. Both waves propagated eastward with a phase speed of about 12 m s⁻¹, the first one decaying rapidly after reaching about 100°E. The first wave appears to disappear at about 115°E based on the rainfall data, but a dynamical component may have continued moving eastward, coupling with convection at about 120°E. The second wave, in contrast, strengthened rapidly upon passing Sumatra, and reached as far as 180°, impinging upon and strengthening an MJO mode already present in the western Pacific.

2.2 Data Assimilation

In order to investigate the wind fields associated with the Kelvin waves, regional analyses were carried out using COAMPS. Data assimilation cycles were run with a 12-h update interval using a double-nested grid. The outer

* Corresponding author address: James A. Ridout, Naval Research Laboratory, Monterey, CA, 93943; email: james.ridout@nrlmry.navy.mil.

nest, with 12-km horizontal grid dimension, uses a parameterized (Kain-Fritsch 1990) treatment of convection. Convection is modeled explicitly on the inner (4-km mesh) grid. The outer grid extends from 60° - 130°E and 26°S - 30°N, and the inner grid extends from 83° - 110°E and 7°S - 11°N. Each grid has 40 levels in the vertical. The update cycle was initiated at 0000 UTC on 14 June for the coarser grid, and 0000 UTC on 17 June for the finer grid. The ending time was 0000 UTC on 23 June for both grids. Although the region of study is only sparsely sampled by conventional observational instruments, a considerable amount of satellite-derived data is ingested in the analyses.

2.3 Forecast Data

In order to investigate the difficulties in modeling Kelvin wave passage past Sumatra, as well as the impact of the Sumatran terrain and surface type (“land” versus “sea”) on the passage of the Kelvin waves, three sets of COAMPS forecasts were carried out. One set of forecasts (“Control”) was run using the above analyses for initial conditions. A second set of forecasts (“Flat Sumatra”) was run in which the Sumatran terrain elevation was set to sea level. A third set of forecasts (“No Sumatra”) was run in which both the Sumatran terrain was removed, and the surface type was set to “sea”. Initial conditions for the modified runs were obtained by running the data assimilation cycle with the modifications incorporated. A fourth set of forecasts (“Explicit Convection”) is briefly examined in section 8.

3. KELVIN WAVE PASSAGE PAST SUMATRA

The date at which the two Kelvin waves pass Sumatra can be estimated from Fig. 1, keeping in mind that the plotted rainfall data correspond to daily averages starting at 0000 UTC on the plotted dates. These data suggest passage by the two waves on 19 June and 21 June,

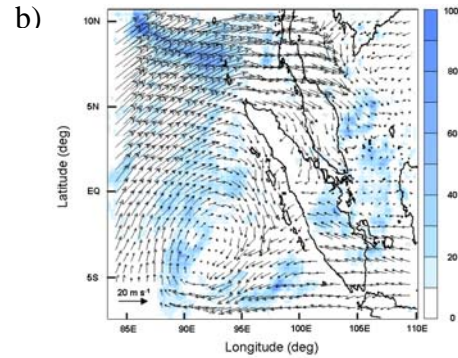
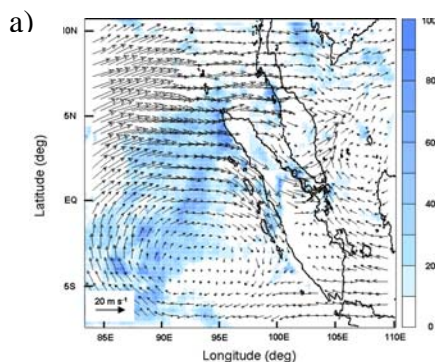


Fig. 2. 850-hPa horizontal wind fields and shaded 24-h TRMM rainfall accumulation (mm) from the 4-km grid analyses on a) 19 June, and b) 21 June.

respectively. The analyzed 850-hPa wind fields at 0000 UTC for these dates on the 4-km COAMPS grid are plotted in Fig. 2 together with the corresponding TRMM rainfall accumulations for the preceding 24-h period. To varying degrees, the plots show a significant amount of rainfall to the west and northwest of Sumatra in a cyclonic vortex and a region of westerly/southwesterly flow. The two wave passages are found to exhibit different patterns of low-level flow past Sumatra. On 19 June, there is flow across the central portion of the island, as well as past the northern tip. A topographic cross section (Fig. 3) shows a gap in the



Fig. 3. Projection of the Sumatran topography onto a north-south vertical plane.

Bukit Barisan mountain range near the equator corresponding to the flow across Sumatra in Fig. 2a. On 21 June, the vortex is tilted from southwest to northeast (Fig. 2b), and the low-level flow eastward past Sumatra is limited to flow around the northern end of the island.

A perspective on the vertical profile of the winds on 19 and 21 June is given in Fig. 4, which shows vertical cross sections of the 4-km grid u-wind component along the 97°E meridian. One sees here the high terrain at the northern end of Sumatra at about 5°N. The flow on 19 June appears to be split, with local maxima in wind speeds to the south and north of the terrain. This splitting is not very evident on 21 June. Further to the east, along the 100°E meridian (Fig. 5), a split in the flow is also observed on 19 June,

whereas the westerly flow on 21 June is mostly limited to the north of the island.

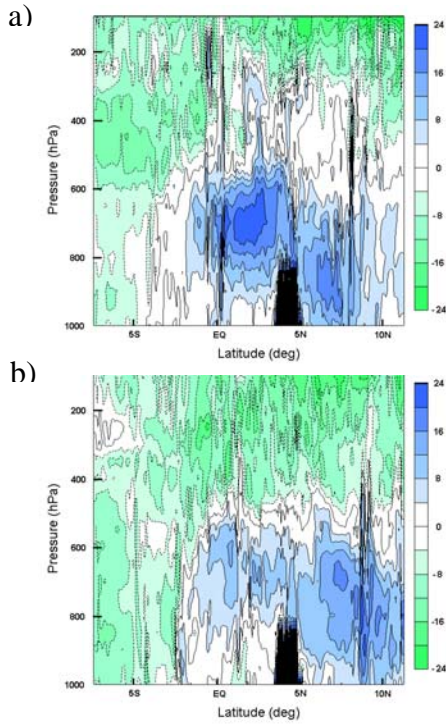


Fig. 4. Vertical cross-section of the u-wind component (m s^{-1}) at 97°E at 0000 UTC on (a) 19 June, and (b) 21 June of 2006 on the 4-km grid.

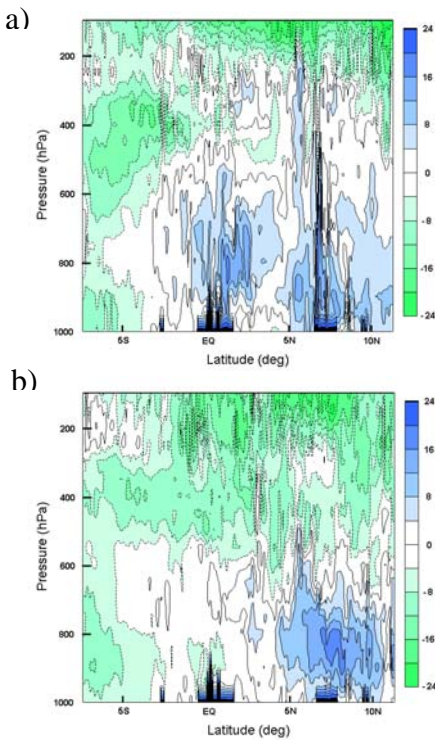


Fig. 5. As in Fig. 4, but at 100°E .

Further downstream, at 107°E , the corresponding vertical cross-sections two days after the Sumatra passages (Fig. 6) are consistent with Fig. 1 in supporting the conclusion that the first wave dissipated, whereas the second wave continued eastward. Note the equatorward propagation of the second wave (Fig. 6b compared with the position in Fig. 4b).

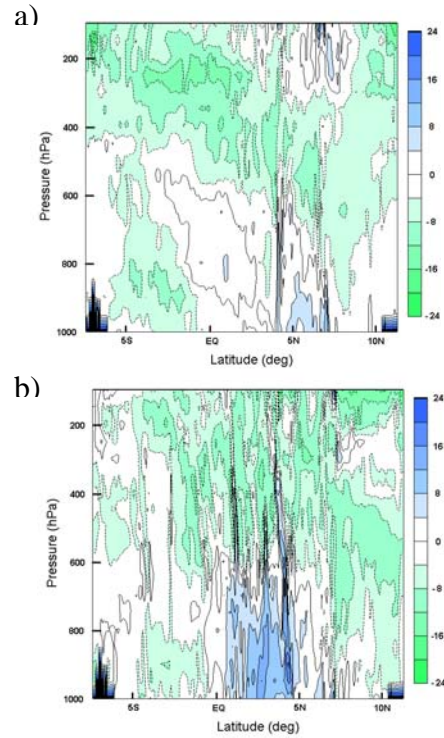


Fig. 6. Vertical cross-section of the u-wind component (m s^{-1}) at 107°E at 0000 UTC on (a) 21 June, and (b) 23 June of 2006 on the 4-km grid.

4. REGIONAL PERSPECTIVE

The presence of mountainous Borneo to the east of Sumatra (Fig. 7) may tend to favor waves that propagate around the northern end of the island rather than primarily over it. This conclusion appears to be consistent at least with the cases examined here.



Fig 7. Sumatra and neighboring islands.

The equatorward propagation of the second equatorial Kelvin wave upon passing Sumatra helped to keep the wave within the latitudinal zone permitting its continued existence. The difference in equatorward propagation of the two waves upon passing Sumatra is evident in both Fig. 2 and in the following day comparison shown in Fig. 8.

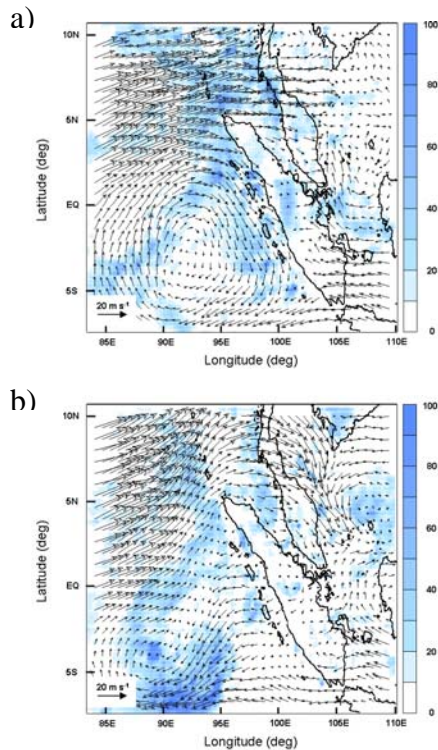


Fig. 8. Same as Fig. 2, but for (a) 20 June, and (b) 22 June.

The equatorward propagation of the second wave was followed by the development of strong convection in an area of convergent low-level flow to the east of Sumatra (not shown).

The manner and frequency of occurrence of flow around the island as seen in Figs. 2b and 8b is a topic for further investigation. In the present case, the large-scale context of the flow is illustrated in Fig. 9, which shows the 850 hPa wind fields on the 12-km grid domain on 18 June and 22 June. In addition to the cyclonic vortex off the west coast of Sumatra, there is a large one as well by 22 June in the Bay of Bengal and the Indian subcontinent. Such a combination has been noted in conjunction with the 10-20-day mode of the Indian monsoon (Chen and Chen 1993).

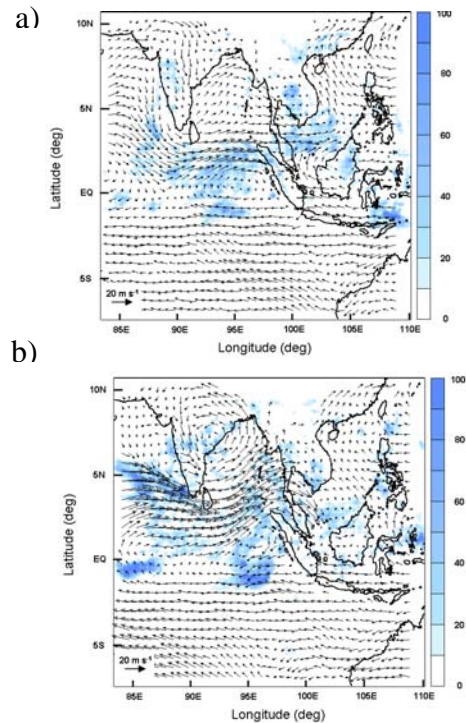


Fig. 9. 12-km grid 850 hPa horizontal winds at 0000 UTC on (a) 18 June and (b) 22 June, 2006, and the TRMM preceding 24-h accumulation (mm) of rainfall.

5. FORECAST EXPERIMENTS

In order to investigate the difficulties in modeling Kelvin wave passage past Sumatra, as well as the impact of the Sumatran terrain and surface type (“land” versus “sea”) on the passage of the Kelvin waves, three sets of COAMPS forecasts were carried out. One set of forecasts (“Control”) was run using the above analyses for initial conditions. A second set of forecasts (“Flat Sumatra”) was run in which the Sumatran terrain elevation was set to sea level. A third set of forecasts (“No Sumatra”) was run in which both the Sumatran terrain was removed, and the surface type was set to “sea”. Initial conditions for the modified runs were obtained by running the data assimilation cycle in the same manner as for the “Control”. A fourth set of forecasts (“Explicit Convection”) is briefly examined in section 8.

6. “CONTROL” FORECAST

The nested grid described in section 2 was employed to simulate the response of the first Kelvin wave to the various treatments of Sumatra. Due to the notable disparity in the forecast skill on the two grids (see below) combined with the limited areal extent of the inner (4-km) mesh domain, only short-term (24-h) forecast comparisons are made here. The

forecast comparison begins with the “Control” forecast and the approach of the first Kelvin wave on 18 June. The 850 hPa horizontal wind analyses on the 4- and 12-km grids for 0000 UTC on this day are shown in Fig. 10, along with the preceding 24-h TRMM rainfall accumulation.

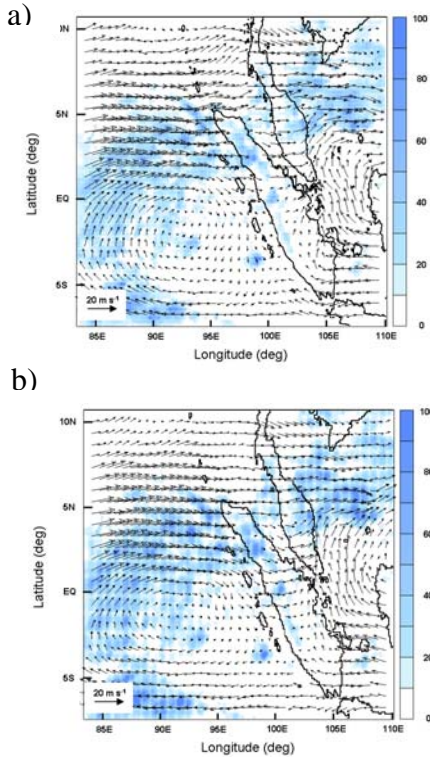


Fig. 10. “Control” 4-km grid (a) and 12-km grid (b) 850 hPa horizontal wind analysis at 0000 UTC on 18 June, 2006, and the preceding 24-h TRMM rainfall accumulation in mm.

One sees that the low-level wind fields at the start of the forecast are very similar for the two grids. This similarity extends to comparisons with the analyses for the “Flat Sumatra” and “No Sumatra” runs (not shown). Figure 11 shows the 24-h forecasts for the 850 hPa wind field made from 0000 UTC on 18 June, and the 24-h forecast rainfall accumulation for the two grids.

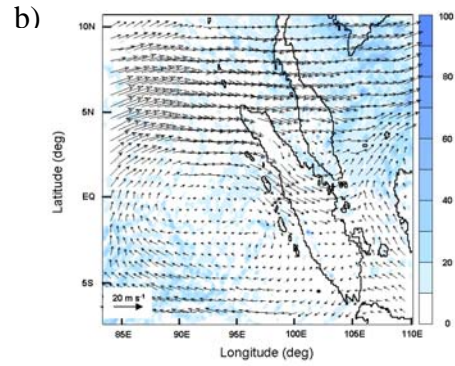
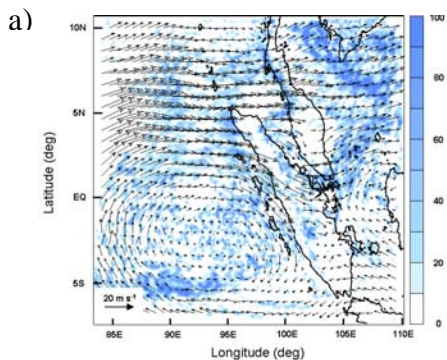


Fig. 11. “Control” 4-km grid (a) and 12-km grid (b) 24-h 850 hPa horizontal wind forecast verifying at 0000 UTC on 19 June, 2006, and the 24-h forecast rainfall accumulation in mm.

The verifying analyses (both 4-km and 12-km) are shown in Fig. 12, together with the 24-h TRMM rainfall accumulation.

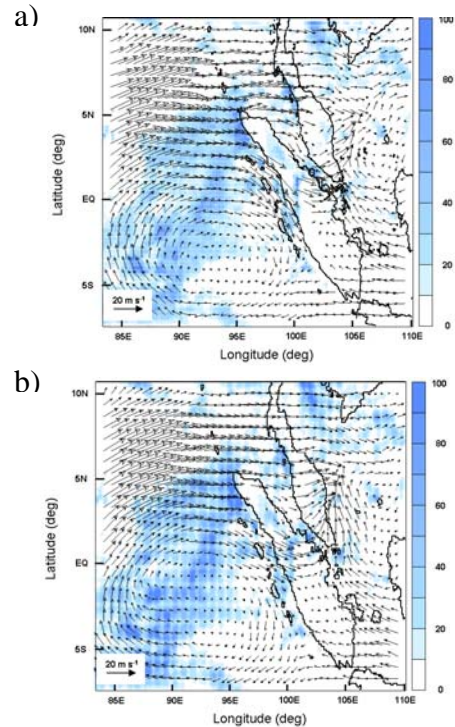


Fig. 12. “Control” 4-km grid (a) and 12-km grid (b) 850 hPa horizontal wind analysis at 0000 UTC on 19 June, 2006, and the preceding 24-h TRMM rainfall accumulation in mm.

Both forecasts predict too much rainfall to the east of Sumatra and the Malay Peninsula, a problem apparently associated with model spinup. The 4-km forecast performs significantly better in representing the rainfall in the westerlies and cyclonic vortex to the west of Sumatra. Note that the vortex is shifted northward on the 12-km grid.

The corresponding plots for the 24-h forecasts verifying at 0000 UTC on 20 June, including the verifying analyses, are shown in Figs. 13 and 14.

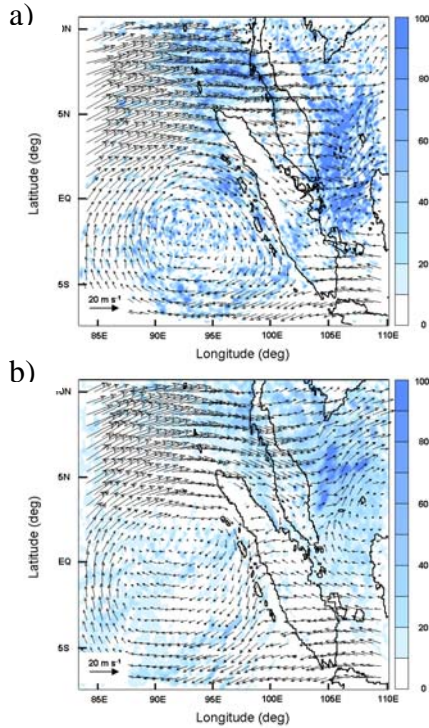


Fig. 13. As in Fig. 11, but for forecasts verifying at 0000 UTC on 20 June, 2006.

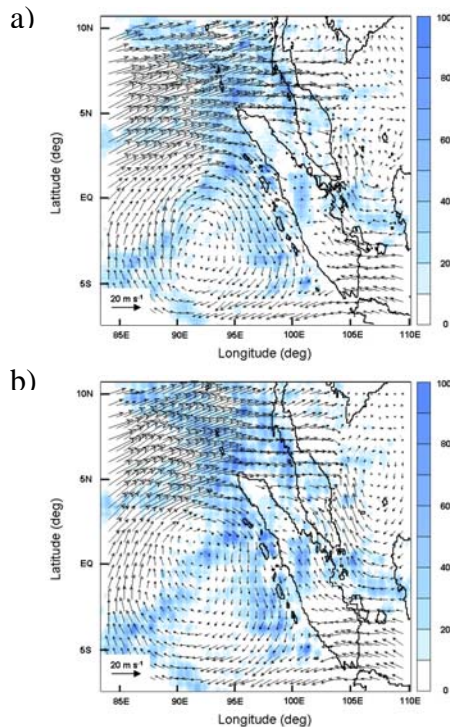


Fig. 14. As in Fig. 12, but for 20 June, 2006.

The relative performance of these 4-km and 12-km forecasts is similar to that noted for the forecasts verifying on 19 June. The 12-km analyses and forecasts place the vortex to the west of Sumatra further to the north than in the 4-km results. Further tests support the conclusion that this difference results from the underrepresentation of latent heating in the vortex on the 12-km grid.

7. SENSITIVITY TO TERRAIN AND SURFACE TYPE

The sensitivity of the Kelvin wave forecasts from 0000 UTC on 18 June on the 4-km grid to the treatment of Sumatra in the model is illustrated in Fig. 15.

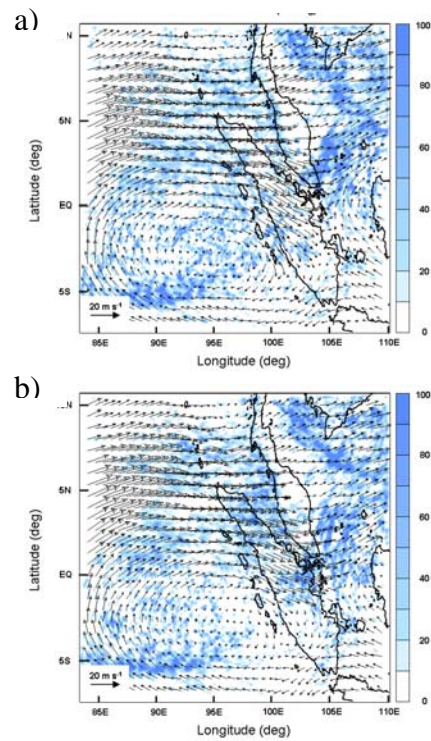


Fig. 15. 4-km grid “Flat Sumatra” (a) and “No Sumatra” (b) 24-h 850 hPa horizontal wind forecast verifying at 0000 UTC on 19 June, 2006, and the 24-h forecast rainfall accumulation in mm.

As one may expect with removal of the mountains, both forecasts in Fig. 15 show more low-level flow over Sumatra than seen in the “Control” (Fig. 11a). The rainfall in the “No Sumatra” run is notably enhanced over the location of Sumatra compared with the other runs and the TRMM data. Note in contrast, the small amount of rainfall over the Malay Peninsula. The present results suggest that by impacting surface fluxes, land features in the Maritime Continent may act to limit convective coupling with

propagating Kelvin waves (in addition to topographical effects, which can act to block the Kelvin wave signal). The vertical profile of the wind forecasts for the “Control” and “No Sumatra” runs at 103°E is plotted in Fig. 16. One finds an enhancement in the strength of the westerly flow along the equator in the “No Sumatra” run, and a decrease to the north of 5°N.

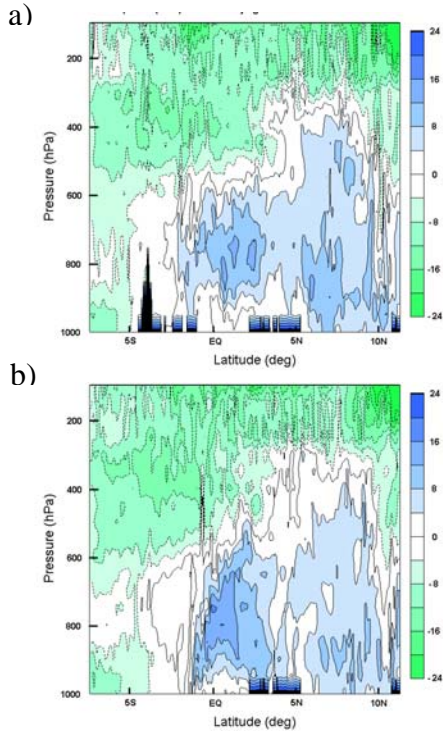


Fig. 16. Vertical cross-section of “Control” (a), and “No Sumatra” (b) 24-h forecast 4-km grid u-wind component (m s^{-1}) at 103°E verifying at 0000 UTC on 19 June.

These simulations suggest that Sumatra enhances the westerly flow past its northern tip during the passage of this Kelvin wave.

Figure 17 shows the 24-h forecasts for the 850 hPa wind field verifying at 0000 UTC on 20 June for the (a) “Flat Sumatra case”, and (b) the “No Sumatra case”.

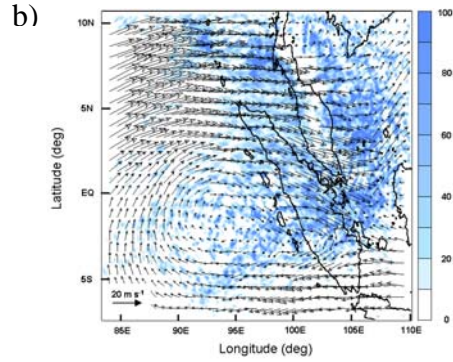
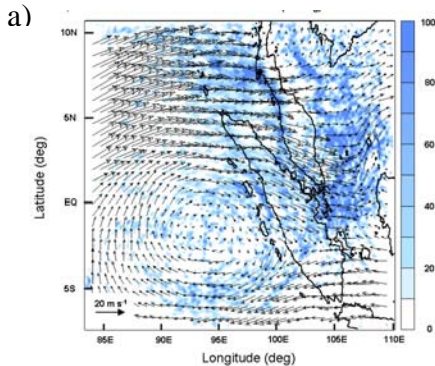


Fig. 17. 4-km grid (a) “Flat Sumatra” and (b) “No Sumatra” 24-h 850 hPa horizontal wind forecasts verifying at 0000 UTC on 20 June, 2006, and the 24-h forecast rainfall accumulation in mm.

In this case, both runs show a rainfall enhancement over Sumatra with respect to the “Control” (Fig. 13a), though it is greatest for the “No Sumatra” run. The vertical profile of the wind forecasts for the “Control” and “No Sumatra” runs at 103°E is plotted in Fig. 18.

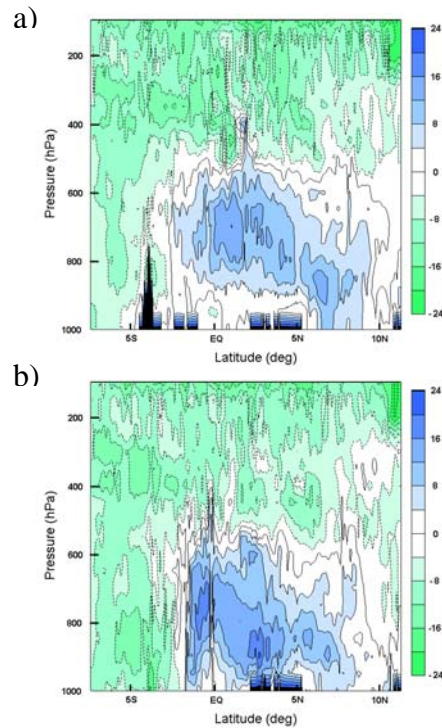


Fig. 18. Vertical cross-section of “Control” (a), and “No Sumatra” (b) 24-h forecast 4-km grid u-wind component (m s^{-1}) at 103°E verifying at 0000 UTC on 20 June.

The impact of Sumatra in this forecast is similar to that observed in Fig. 16.

Looking briefly now at the 12-km grid results, the u-wind vertical profile plots at 103°E for the 18 June forecasts suggest little impact of Sumatra (Fig. 19). This lack of sensitivity is

found as well for the 19 June forecasts (not shown). Based on the better rainfall simulations on the 4-km grid, the

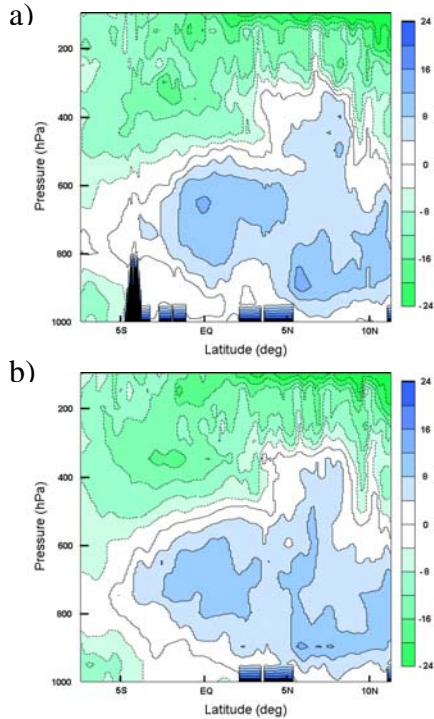


Fig. 19 As in Fig. 16, but for the 12-km grid.

Sumatra impact demonstrated in Fig. 16 seems more probable than the lack of impact in Fig. 19. This conclusion is also supported by comparing the “Control” forecast results for the two grids (Fig. 16a and Fig. 19a) with the corresponding analyses in Fig. 20. A notable difference between the forecasts is that on the coarser grid in the equatorial zone, the westerly flow is strongest approximately 100 hPa higher up than on the 4-km grid. In general, the westerly flow on the 4-km grid is stronger closer to the surface than on the 12-km grid. These differences may reflect the lack of a treatment for convective momentum transport in the Kain-Fritsch scheme used here on the 12-km grid (Houze et al. 2000).

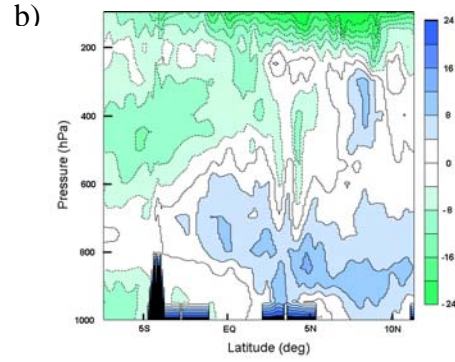
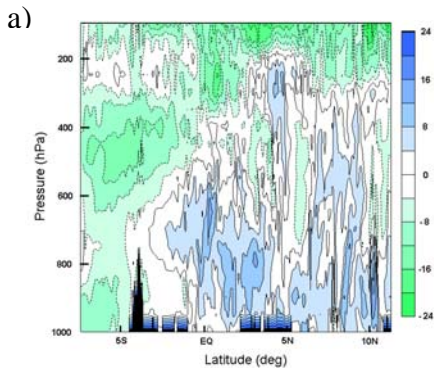


Fig. 20. Vertical cross-section of “Control” 4-km grid (a), and 12-km grid (b) u-wind component (m s⁻¹) at 103°E at 0000 UTC on 19 June.

8. LARGE-SCALE IMPLICATIONS

By expanding the focus domain and considering more cases, further progress towards understanding propagation of equatorial Kelvin waves and the MJO through the Maritime Continent may be achieved, as well as implications for the Indian monsoon (cf. Maloney and Hartmann 1998). Unfortunately, deficiencies in the simulation of the flow on the 12-km grid preclude inference of large-scale implications from the present results. To test the sensitivity of the noted deficiencies to the representation of convection, 72-h forecasts (Fig. 21) were carried

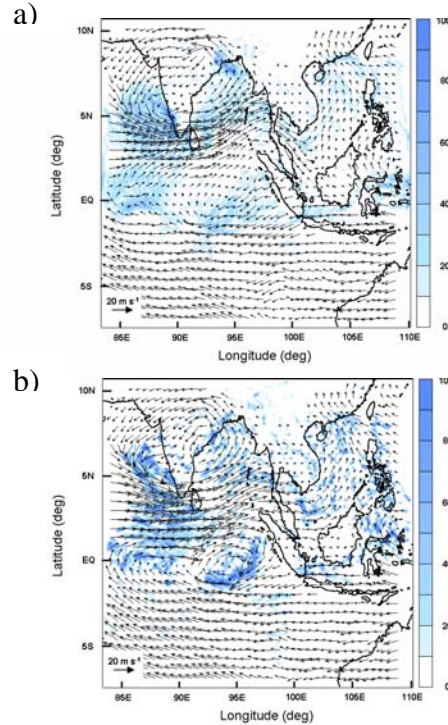


Fig. 21. “Control” (a) and “Explicit Convection” (b) 12-km grid 72-h forecast 850 hPa winds verifying at 0000 UTC on 22 June, and the final 24-h of forecast rainfall accumulation in mm.

out for the “Control” and a model version (“Explicit Convection”) in which convection is represented explicitly on the 12-km grid. Although 12-km is extremely coarse for explicit simulation of convection, the “Explicit Convection” forecast appears to validate best (see Fig. 9b). Some key deficiencies may be noted, nonetheless, including the representation of the flow around Sumatra. The turning of the flow around the island (Figs 2b and 8b) suggests that generation of vorticity further west through convective heating may be a key factor for propagation past Sumatra. One sees in Fig. 21, that the two convective treatments differ considerably in this respect. In a different context, tropical cyclones, the contribution of convective heating to vorticity production which aids passage around mountains, has been previously described (Chang 1982).

9. DISCUSSION AND CONCLUSIONS

The present forecast experiments highlight the importance of a realistic representation of deep convection in simulating the interaction of equatorial Kelvin waves (and presumably the MJO) with Sumatra. The analyses and TRMM rainfall data presented for June 2006 suggest that the island represents a significant barrier to propagation of such waves. This factor may explain the apparent dissipation (or transformation associated with MJO development) of an equatorial Kelvin wave in the eastern Indian Ocean in May 1998 noted by Straub et al. (2006), an episode consistent in some respects with a composite presented in the same study from 25 years of data showing a pair of equatorial Kelvin waves associated with the onset of the South China Sea summer monsoon. Successful passage past Sumatra (including subsequent propagation past Borneo) may be favored for waves in which the low-level flow passes around the northern end of Sumatra, as in the second wave examined here, rather than being split, partly passing over the central portion of the island. The passage around the island in the second wave may have been aided by vorticity production associated with deep convection in the cyclonic vortex to the west of Sumatra. Regarding the mode of impact of Sumatra in the case of the “split” Kelvin wave examined here, the forecast experiments support both a significant terrain blocking effect, as well as a disruption of favorable coupling of the wave with surface fluxes that occurs over the ocean. The combined effect is for the island to significantly reduce the equatorial westerly flow and accompanying deep convection.

Acknowledgments. The rainfall data used in this study were acquired using the GES-DISC Interactive Online Visualization AND aNalysis

Infrastructure (Giovanni), a part of the NASA Goddard Earth Sciences (GES) Data and Information Services Center (DISC). This research was sponsored by the Naval Research Laboratory under Program Element 0601153N. The work was supported in part by a grant of computing time from the Department of Defense’s High Performance Computing Program.

REFERENCES

- Chang, S. W.-J., 1982: The orographic effects induced by an island mountain range on propagating tropical cyclones. *Mon. Wea. Rev.*, **110**, 1255-1270.
- Chatterjee, P., and B. N. Goswami, 2004: Structure, genesis and scale selection of the tropical quasi-biweekly mode. *Q. J. R. Meteorol. Soc.*, **130**, 1171-1194.
- Chen, S. S., R. A. Houze, Jr., and B. E. Mapes, 1996: Multiscale variability of deep convection in relation to large-scale circulation in TOGA COARE. *J. Atmos. Sci.*, **53**, 1380-1409.
- _____, et al., 2003: COAMPS version 3 model description - general theory and equations. Naval Research Laboratory Technical Report, NRL/PU7500-04-448. 141 pp.
- Chen, T.-C., and J.-M. Chen, 1993: The 10-20-day mode of the 1979 Indian monsoon: Its relation with the time variation of monsoon rainfall. *Mon. Wea. Rev.*, **121**, 2465-2482.
- Gill, A., 1980: Some simple solutions for heat-induced tropical circulation. *Q. J. R. Meteorol. Soc.*, **106**, 447-462.
- Hayashi, Y.-Y., and A. Sumi, 1986: The 30-40 day oscillations simulated in an “aquaplanet” model. *J. Meteorol. Soc., Jpn.*, **64**, 451-466.
- Hendon, H., 1988: A simple model of the 40-50 day oscillation. *J. Atmos. Sci.*, **45**, 569-584.
- Hodur, R. M., 1997: The Naval Research Laboratory’s Coupled Ocean/ Atmosphere Mesoscale Prediction System (COAMPS). *Mon. Wea. Rev.*, **125**, 1414-1430.
- Hogan, T. F., T. E. Rosmond, and R. Gelaro, 1991: The NOGAPS forecast model: A technical description. NOARL Report 13. Naval Research Laboratory (formerly NOARL), Monterey, CA.
- Houze, R. A., et al., 2000: Convection over the Pacific warm pool in relation to the atmospheric KR Wave. *J. Atmos. Sci.*, **57**, 3058-3089.
- Inness, P. M., and J. M. Slingo, 2006: The interaction of the Madden-Julian Oscillation with the Maritime Continent in a GCM. *Q. J. R. Meteorol. Soc.*, **132**, 1645-1667.
- Kain, J. S., and M. Fritsch, 1990: A one-dimensional entraining/detraining plume model and its application in convective

- parameterization. *J. Atmos. Sci.*, **47**, 2784-2802.
- Madden, R., and P. Julian, 1971: Detection of a 40-50 day oscillation in the zonal wind in the tropical Pacific. *J. Atmos. Sci.*, **28**, 702-708.
- _____, and _____, 1972: Description of global scale circulation cells in the Tropics with a 40-50 day period. *J. Atmos. Sci.*, **29**, 1109-1123.
- _____, and _____, 1994: Observations of the 40-50 day tropical oscillation--- A review. *Mon. Wea. Rev.*, **122**, 814-837.
- Maloney, E. D., and D. L. Hartmann, 1998: Frictional moisture convergence in a composite life cycle of the Madden-Julian Oscillation. *J. Climate*, **11**, 2387-2403.
- Simpson, J., R. F. Adler, and G. R. North, 1988: Proposed Tropical Rainfall Measuring Mission (TRMM) satellite. *Bull. Amer. Meteor. Soc.*, **69**, 278-295.
- Straub, K. H., G. N. Kiladis, and P. E. Ciesielski, 2006: The role of equatorial waves in the onset of the South China Sea summer monsoon and the demise of El Niño during 1998. *Dyn. Atmos. Oceans*, **42**, 216-238.
- Zhang, C., 2005: Madden-Julian Oscillation. *Rev. Geophys.*, **43**, RG2003, doi:10.1029/2004RG000158.